ACS APPLIED MATERIALS & INTERFACES

Research Article

www.acsami.org

Noncovalently Functionalized Multiwalled Carbon Nanotubes by Chitosan-Grafted Reduced Graphene Oxide and Their Synergistic Reinforcing Effects in Chitosan Films

Yongzheng Pan, Hongqian Bao, and Lin Li*

School of Mechanical and Aerospace Engineering, Nanyang Technological University, 50 Nanyang Avenue, Singapore 639798

Supporting Information

ABSTRACT: Water-soluble chitosan-grafted reduced graphene oxide (CS-rGO) sheets are successfully synthesized via amidation reaction and chemical reduction. CS-rGO possesses not only remarkable graphitic property but also favorable water solubility, which is found to be able to effectively disperse multiwalled carbon nanotubes (MWCNTs) in acidic solutions via noncovalent interaction. The efficiency of CS-rGO in dispersing MWCNTs is tested to be higher than that of plain graphene oxide (GO) and a commercial surfactant, sodium dodecyl sulfate (SDS). With incorporation of 1 wt % CS-rGO dispersed MWCNTs (CS-rGO-MWCNTs), the tensile modulus, strength and toughness of the chitosan (CS) nanocomposites can be increased by 49, 114, and 193%, respectively. The reinforcing and toughening effects of CS-rGO-MWCNTs are much more prominent than those of single-component fillers, such as MWCNTs, GO, and CS-rGO. Noncovalent $\pi-\pi$ interactions between graphene sheets and nanotubes and hydrogen bonds between grafted CS and the CS matrix are responsible for generating effective load transfer between CS-rGO-MWCNTs and the CS matrix, causing the simultaneously increased strength and toughness of the nanocomposites.

KEYWORDS: *reduced graphene oxide, multiwalled carbon nanotubes, noncovalent, chitosan, nanocomposites, mechanical properties*

1. INTRODUCTION

Graphene, two-dimensional (2D) single or few layers of sp^2-bonded carbon sheets, has attracted a great deal of interest in the past few years owing to its exceptional physical properties.[1−3] In preparation of graphene sheets, the method of utilizing exfoliated graphene oxide (GO) sheets as precursors has been widely used.[4−6] GO is an oxidized form of graphene with phenol hydroxyl and epoxide groups on the basal plane and carboxylic groups at the edges, and normally produced through processing graphite under oxidative conditions. Due to the abundant oxygen-containing groups, GO is soluble in water and some polar solvents. Besides, it can be readily converted into chemically reduced graphene oxide (rGO) by reducing agents in solutions. This provides an economic and convenient approach to fabrication of various desired materials such as paper-like materials,[7] coatings,[8] composites,[9] based on GO and graphene through solution-based techniques. Because of its cost-effectiveness, massive scalability, versatility for functionalization, and easy processability, the colloidal route based on GO is regarded as one of the most attractive and promising options for many potential applications of graphene.

GO has been described as a hydrophilic material since its discovery because of its excellent water solubility. Its surfactant-like characteristic at interfaces has been reported recently and studied intensely.[10−17] GO has not only hydrophilic groups on the edges but also a largely hydrophobic basal plane, so that it should be viewed as an amphiphile and act like a surfactant. Zhao et al.[18] and Zhang et al.[19] respectively reported the synthesis of polystyrene (PS) colloidal particles stabilized by GO sheets through emulsion polymerization based on Pickering emulsion. GO sheets are able to stabilize PS colloidal particles in an aqueous solution for several weeks. Sharif et al. prepared GO/poly(methyl methacrylate) (PMMA) composite using the similar method.[15] It is indicated that GO is potentially able to be utilized as a replacement for traditional surfactants in emulsion polymerization. In addition, it provides a facile way to produce water-based and surfactant-free GO/polymer composites with high performance. On the other hand, because GO can be cleanly converted to rGO, it is possible to create carbon−carbon interface in the final composite by using GO as a dispersant for carbon materials like graphite, carbon black and carbon nanotubes, thus opening up new ways to make all-carbon hybrid materials with diverse functionalities. Sun et al. have found that GO sheets were highly effective in dispersing both as-purified and separated semiconducting single-walled carbon nanotubes (SWCNTs).[20] The aqueous GO/SWCNT dispersion can be used to fabricate transparent conductive coating by a simple air-spray method. Huang et al. discovered

Received: September 26, 2011
Accepted: November 17, 2011
Published: November 17, 2011

   dx.doi.org/10.1021/am2013135 | ACS Appl. Mater. Interfaces 2011, 3, 4819–4830

that GO can act as an emulsifier to generate stable oil droplets in water and as a dispersant to disperse graphite, fullerenes (C_{60}), as well as carbon nanotubes in water.[11,12] The C_{60}/SWCNT/GO composites prepared via the colloidal route exhibited an unprecedented photoconductive response with a high power conversion efficiency.

However, the efficiency of GO to disperse carbon nanotubes (CNTs) is still limited because the basal plane of GO is not graphitic enough due to the epoxide and hydroxyl groups. Liu et al. reported that GO could hardly disperse and stabilize multiwalled carbon nanotubes (MWCNTs) effectively if GO/MWCNT mass ratio was less than 1.[16] If we can make the basal plane of GO more graphitic by removing those oxygen-containing groups on basal planes of GO sheets, it should be able to disperse CNTs more efficiently. A straightforward method is to reduce GO to rGO.[12] Unfortunately, rGO tends to agglomerate and precipitates in aqueous solutions upon reduction because of the decrease of hydrophilic character,[21] making it less ideal for the purpose. To make stable dispersions of rGO, it is necessary to functionalize GO with water-soluble polymers prior to the chemical reduction. So far, there has been plenty of work focusing on functionalization of rGO with various polymers by covalent or noncovalent methods, which provides a variety of routes to produce rGO derivatives soluble in water or organic solvent.[22−24] The polymers for functionalization of rGO include amphiphilic polymers,[25] polyeletrolytes,[26] vinyl polymers,[27,28] conjugated polymers,[29] biocompatible polymers,[30,31] as well as polyolefin.[32] These polymer-functionalized rGO sheets possess not only excellent solubility in water or other proper solvents but also fully graphitic basal planes. By taking advantage of the progress, it is possible to develop rGO-derivatives with higher efficiency in dispersing and stabilizing CNTs. However, to the best of our knowledge, there have been no works to date that were dedicated to developing functionalized rGO for dispersing CNTs and then fabricating hybrid materials based on rGO/CNT complexes.

Recently, we have synthesized several kinds of water-soluble functionalized graphene sheets and studied their applications in drug loading and delivery.[33−35] Because of the strong noncovalent interactions between graphene and drugs, these graphene sheets exhibited high efficiency in binding drugs. In this work, we employed a covalent method to graft chitosan (CS), a natural water-soluble polymer, onto the GO surface followed by chemical reduction, and thus obtained chitosan-grafted graphene sheets (CS-rGO). The CS-rGO possessed both a remarkably graphitic property and a favorable water solubility. On account of its amphiphilic property, CS-rGO is able to disperse MWCNTs in acidic solutions via $\pi-\pi$ interaction and hydrophobic interaction. The efficacy of CS-rGO in dispersing MWCNTs was evaluated with UV−vis absorption spectra, and CS-rGO dispersed MWCNTs were observed by transmission electron microscopy (TEM) and atomic force microscopy (AFM). We also compared the ability of CS-rGO to disperse MWCNTs with that of plain GO and sodium dodecyl sulfate (SDS). Afterward, the CS-rGO dispersed MWCNTs (CS-rGO-MWCNTs) were incorporated into a chitosan matrix, and the prepared nanocomposites exhibited simultaneous increases in both strength and toughness. The mechanical properties of CS-rGO-MWCNT/CS nanocomposites were found to be significantly higher than those containing single-component fillers like plain GO, MWCNTs and CS-rGO.

2. EXPERIMENTAL SECTION

2.1. Materials. Graphite with an average particle size of 100 μm was obtained from Fluka. Chitoan (M_n = 3 kDa) with 90% degree of deacetylation (DD, determined by ^{1}H NMR) was provided by Haidebei Marline Bioengineering Co., Ltd., China. MWCNTs were purchased from Iljin Nano Tech, Korea. Their diameter and length were about 10−15 nm and 10−20 μm, respectively. MWCNTs were purified by thermal oxidation (350 °C for 2 h in air) and acid treatment (refluxing in 6 M HCl solution for 12 h) before use. 2-(*N*-Morpholino)ethanesulfonic acid (MES, 99%), *N*-(3-dimethylaminopropyl)-*N*′-ethylcarbodiimide hydrochloride (EDC·HCl, 99%) and *N*-hydroxysuccinimide (NHS, 97%) were obtained from Aldrich and directly used. Other reagents mentioned in this article were purchased from Aldrich and used as received.

2.2. Synthesis of CS-rGO. GO was synthesized from graphite powder by a modified Hummers method.[36−38] CS-rGO precursor was synthesized by the amidation of GO with CS in the presence of EDC and NHS. In a typical procedure, CS (0.5 g, 2.77 mmol) and GO (0.1 g, 0.17 mmol) were first dispersed in 50 mL of MES buffer (0.1 M, pH adjusted to 5) and sonicated for 1 h to get a homogeneous colloidal suspension. Being protected by argon, EDC (0.652 g, 3.4 mmol) and NHS (0.782 g, 6.8 mmol) were gradually charged into the flask within 20 min. The reaction was conducted at room temperature under bath sonication for 6 h and stirring for another 16 h. After the reaction was terminated, the suspension was filtered over a 0.2 μm Nylon microporous membrane and thoroughly washed with a large amount of acetic acid solution (0.1 M) to remove unreacted CS. Thereafter, the collected solid was redispersed and dialyzed (MWCO = 8 kDa) against deionized (DI) water for 3 days at 4 °C. The obtained chitosan grafted graphene oxide (CS-GO) was lyophilized and the yield was about 95% (0.29 g). The CS-GO suspension of a specific concentration was obtained by sonication of the prepared CS-GO in DI water and its pH value was adjusted to 4 by adding acetic acid. L-ascorbic acid (vitamin C) powder of the same weight as CS-GO was subsequently added to the CS-GO suspension, and the mixture was held at 90 °C for 6 h to reduce the CS-GO to CS-rGO. This solution was kept at room temperature overnight to ensure complete reduction and then dialyzed overnight to remove excess L-ascorbic acid. The dialyzed CS-rGO solution was then lyophilized and the dried CS-rGO was obtained for further characterization and application.

2.3. Preparation of CS-rGO/MWCNT Dispersions. A certain amount of CS-rGO was dissolved in acetic acid solutions at different pH values by sonication for 5 min. CS-rGO/MWCNT dispersions were prepared by mixing a certain amount of MWCNTs and 10 mL of CS-rGO solutions with corresponding concentrations, after which the resulting mixtures were sonicated for 30 min. The initial MWCNT concentration was 0.5 mg/mL. All sonication processes were carried out with a tip sonicator (Sonic Vibracell VC750) with a probe of a diameter 10 mm using a fixed output power of 30 W. The sample beaker was placed inside an ice−water bath during sonication in order to prevent rising of the temperature of the mixtures.

2.4. Preparation of CS Nanocomposite Films. The 1 wt % chitosan solution was prepared by dissolving chitosan in 2% (v/v) aqueous acetic acid solution using a magnetic stirrer at 200 rpm for 1 h and filtered with a filter paper to remove the impurity under vacuum. Subsequently, a desired amount of 0.1 mg/mL nanoparticle suspension such as CS-MWCNTs, CS-rGO and CS-rGO-MWCNTs, was added into the chitosan solution. Here, for CS-rGO-MWCNTs, the mass ratio of rGO to MWCNTs was 1:1. The solution was then stirred at 200 rpm for 1 h, followed by sonication for 10 min to remove bubbles. After that, the nanocomposite suspension containing 1 wt % nanoparticles was poured into a plastic dish and placed in fume hood at room temperature to allow water to evaporate to form a film, followed by drying in a vacuum oven at 50 °C for 24 h. The films prepared were cut into test samples using a razor blade and kept in an oven at 50 °C for 2 h before mechanical testing. The preparation method for pristine MWCNT/CS films was shown in the Supporting Information.

Scheme 1. Synthesis Route of CS-rGO

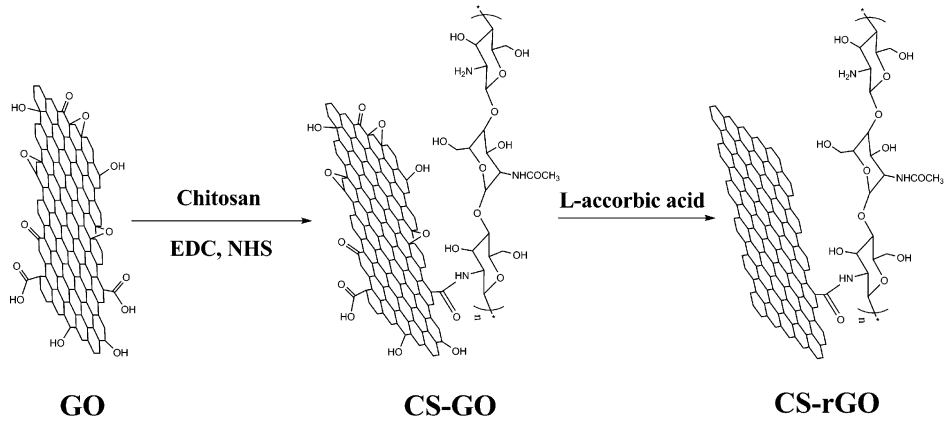

2.5. Characterization. Fourier transform infrared (FTIR) spectra were recorded on a Nicolet 5700 FTIR instrument with attenuated total reflectance (ATR) accessory. UV−vis absorption spectra of GO, CS-GO and CS-rGO were recorded with a Shimadzu UV-3101PC spectrometer. Raman spectra were measured on a Renishaw inVia Raman microscope 2000 with 633 nm laser excitation. For chemical composition analysis, a Kratos Ultra X-ray photoelectron spectroscopy (XPS) system was used with a monochromatic Al Ka X-ray source operating at 15 kV and 10 mA. The core level spectra were obtained at a photoelectron takeoff angle of 90°, measured with respect to the sample surface. Zeta potential analyses were performed using a Malvern Zetasizer Nano instrument and all data were averaged over three times of measurements. UV−vis absorption spectra of dispersed MWCNTs were recorded with a Shimadzu UV-3101PC spectrometer operating from 190 to 800 nm. Samples containing a dispersant and MWCNTs were taken after the sonication in Step 2.3 and treated by centrifugation at 3500 rpm for 15 min to remove the nondispersed nanotubes. Then, the supernatants were diluted by 100 times, resulting in the MWCNT dispersions suitable for UV−vis measurements. The reference was the sole dispersant solution treated under the same conditions as those for the tested samples. Transmission electron microscopy (TEM) observations of MWCNT dispersions were performed using a JEOL JEM-2010 operated at 200 kV. Samples were prepared by dipping a copper TEM grid in the MWCNT dispersion and subsequent drying. Atomic force microscopic (AFM) measurements with the typical tapping-mode were performed using Digital Instrument S3000 AFM. Samples for AFM were prepared by dropping an aqueous GO or CS-rGO solution (~0.01 mg/mL) onto a fresh silicon wafer, followed by drying under ambient conditions for 24 h. The tensile properties of cast samples (dimension 20 mm × 5 mm with varying thickness) were measured using an Instron Model 5543 mechanical tester at room temperature. A 100 N load cell was used and the strain rate was 5.0 mm/min. To ensure data accuracy and repeatability, at least 5 measurements were carried out for each nanocomposite. The morphology of nanocomposite films was observed using field emission scanning electron microscopy (FESEM, JEOL JSM-6700F). Samples were fractured in liquid nitrogen, and sputtered with gold before observation. Raman spectra of the composites under different strains were obtained using a Renishaw inVia Raman microscope 2000 equipped with a 633 nm laser exitation. The composite specimen was loaded in tension with a homemade tensile device and strain was measured using a strain gauge attached to the specimen.

3. RESULTS AND DISCUSSION

3.1. Characterization and pH Responsive Behavior of CS-rGO. As shown in Scheme 1, CS was grafted onto GO surface via amidation reaction according to the procedure in our previous work.[34] Relatively low molecular weight CS (M_n = 3 kDa) was chosen to avoid possible cross-link and excess of CS was used to guarantee a nearly complete consumption of carboxylic groups on GO sheets. The resultant CS-GO was then chemically reduced to CS-rGO by L-accorbic acid. Only under acid conditions CS can be dissolved. Conventional reducing agents such as hydrazine and $NaBH_4$ are all alkaline. L-accorbic acid has been reported as an effective reducing agent which can compete with hydrazine,[39,40] thus it was selected to convert CS-GO to CS-rGO.

FTIR spectral comparison provides the information confirming the successful attachment of CS to the surface of graphene sheets and the chemical reduction from CS-GO to CS-rGO (Figure 1). In Figure 1a, the peaks around 1726 cm^{-1} were

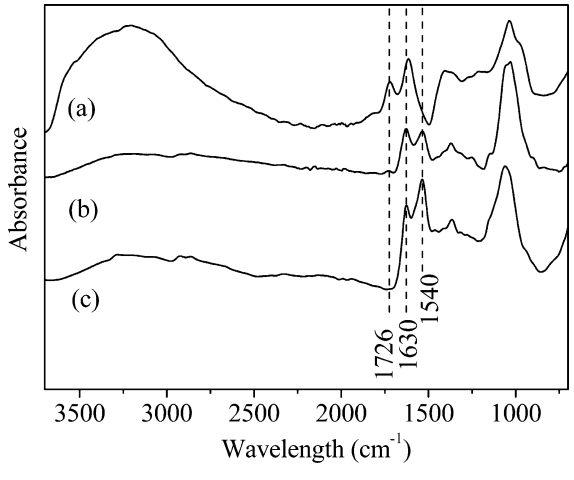

Figure 1. FTIR spectra of (a) GO, (b) CS-GO, and (c) CS-rGO.

characteristic of the C═O in carboxylic acid and carbonyl moieties on the surface of GO. In both of the CS-GO and CS-rGO spectra (Figure 1b, c), the characteristic signals for C═O stretching band of the amide groups at 1630 cm^{-1} and N−H bending of secondary amide at 1540 cm^{-1} indicate the presence of newly formed amide bonds between graphene sheets and CS. Moreover, a small absorbance peak of CS-GO around 1726 cm^{-1} can be discerned, which is attributed to the residual carbonyl moieties (C═O) on the periphery of GO. After being reduced to CS-rGO, these residual carbonyl moieties were removed, thus the absorbance peak of at 1726 cm^{-1} disappeared in the CS-rGO spectrum.

After CS-GO was reduced to CS-rGO, the color of the colloidal dispersion changed from brown to black, which is

similar to the phenomenon during conversion from GO to graphene. From the UV−vis spectra shown in Figure 2A, GO

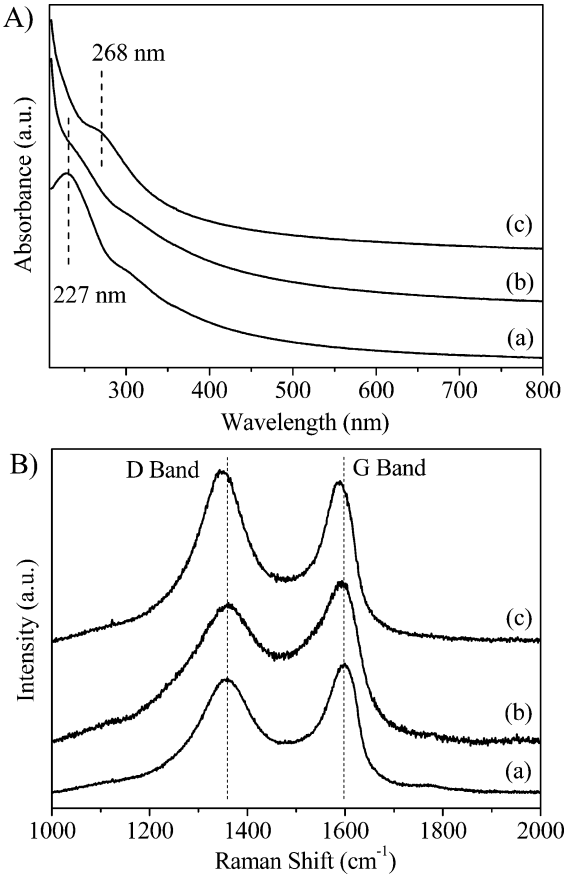

Figure 2. (A) UV−vis spectra and (B) Raman spectra of (a) GO, (b) CS-GO, and (c) CS-rGO.

dispersion demonstrates an absorption peak centered at 227 nm (attributed to the $\pi-\pi^*$ transitions of C−C bonds) and a shoulder peak at 300 nm (attributed to the n-π^* transitions of C═O bonds).[41,42] CS-GO shows the similar spectra with those of GO, indicating the CS grafting did not change the structure of GO basal plane. In contrast, the absorption peak of CS-rGO slightly red-shifted to 268 nm, suggesting that the electronic conjugations within the graphene sheets were partially restored, which is the same as the results of rGO reduced by L-accorbic acid done by Paredes et al.[39] The significant structural changes occurring during chemical reduction are also reflected in the Raman spectra (Figure 2B). In the Raman spectra of GO and CS-GO, the G bands located at 1598 cm^{-1}, which are higher in intensity than D bands at 1358 cm^{-1}. After chemical reduction, both G and D bands of CS-rGO shifted to 1588 and 1348 cm^{-1}, respectively. Moreover, the intensity of D band becomes higher than that of G band. That is to say, the D/G intensity ratio increased. According to the report from Stankovich et al of the Ruoff group,[4] the increase in D/G intensity ratio is because the new graphitic domains created during the reduction of GO to rGO are smaller in size than the size of GO before reduction. Therefore, the decreased average size of rGO makes the D/G intensity ratio increase.

To further verify the reduction of GO in this work, XPS was applied to characterize the surface chemical composition of GO, CS-GO and CS-rGO. The C 1s peaks of the high-resolution XPS spectra obtained are shown in Figure 3. For the spectrum of GO (Figure 3A), the peak at 284.6 eV originates

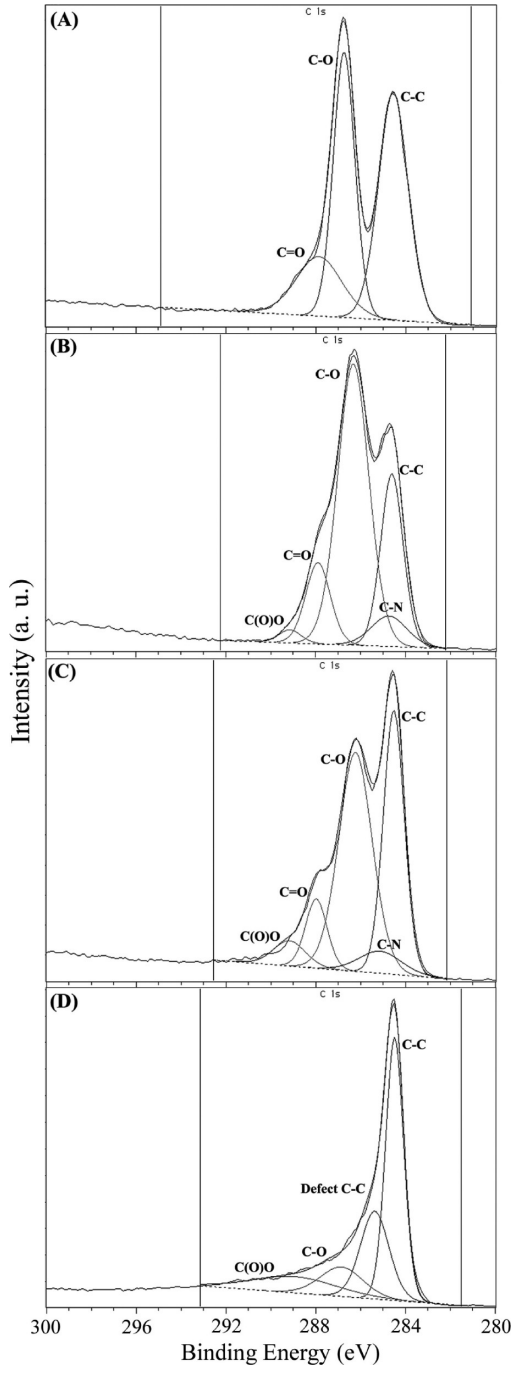

Figure 3. High-resolution XPS spectra of C 1s for (A) GO, (B) CS-GO, (C) CS-rGO, and (D) bare rGO.

from graphitic sp^2 carbon atoms (C−C bond), whereas the one at 286.6 eV is attributed to C−O bond in hydroxyl and epoxide groups and also possibly to C−C bonds in defected structures. The peak located at 287.9 eV is due to carbon atoms in C═O bond, i.e., carbonyl groups.[39] As compared with the spectrum of GO, an additional component at 284.9 eV, which is corresponding to C−N bond, is observed in the C1s XPS spectrum of CS-GO (Figure 3B), which originates from C−N bonds in the grafted CS. Meanwhile, the C−O peak intensity increases remarkably due to abundant C−O bonds in CS.

dx.doi.org/10.1021/am2013135 | ACS Appl. Mater. Interfaces 2011, 3, 4819−4830

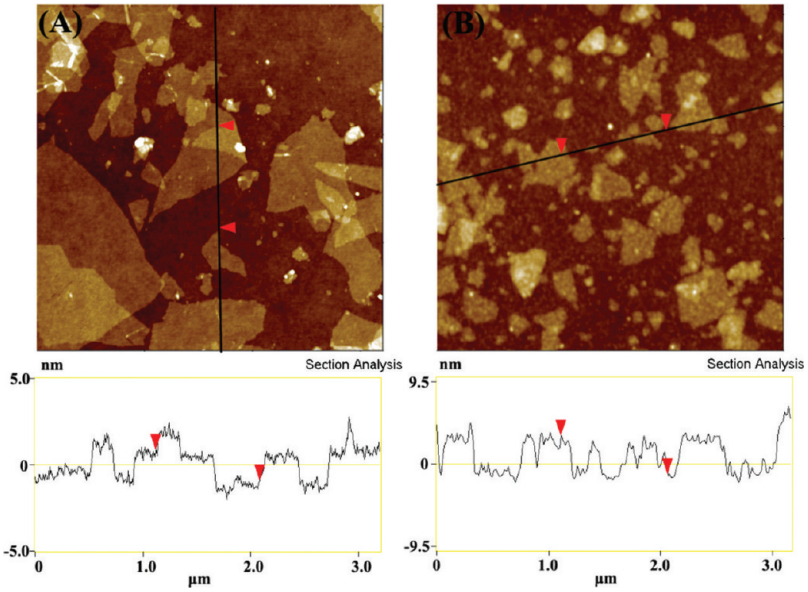

Figure 4. Tapping mode AFM images for (A) GO and (B) CS-rGO.

Figure 3C displays the C1s XPS spectrum of CS-rGO, in which the peak intensities of all oxidized carbon bonds become much lower than the C−C peak intensity, because most of the oxygen-containing groups in GO have been removed after chemical reduction. The residual C−O and C═O bonds are mainly from the grafted CS. We also obtained the XPS spectrum (Figure 3D) of the bare rGO that was reduced under the same condition in order to prove the reducing effectiveness. The peak intensities of all the carbon binding to oxygen decrease significantly and the defect C−C component (285.5 eV) can be discriminated as a characteristic peak of rGO reduced by L-ascorbic acid.[39] The atomic contents of C, O, and N elements in various samples are listed in Table S1 in the Supporting Information. Through calculation, we can find that the rGO component in CS-rGO (excluding the grafted CS) has the C/O atomic ratio of 8.07, close to 8.26, the C/O atomic ratio of bare rGO, suggesting that the reduction of GO was not influenced by grafted CS and almost completely accomplished. Furthermore, the atomic content of N in CS-rGO is close to that in CS-GO. Because the entire N element originates from CS, it indicates that the grafted CS was stable during the reduction process. The FTIR, UV−visible, Raman and XPS results together led to the conclusion that CS was grafted onto the surface of GO and CS-GO was successfully converted into CS-rGO after the chemical reduction.

AFM provides a direct method to characterize the morphology and thickness of GO and CS-rGO sheets. As shown in Figure 4, pristine GO sheets exist as micrometer-sized platelets, while functionalized rGO sheets have sizes in the range of hundred-nanometers due to the sonication treatment and chemical reduction as we mentioned before. The measured thickness of GO sheets is very uniform (~1−1.6 nm), which is consistent with those in the previous reports, suggesting the complete exfoliation of GO sheets down to individual or bilayer ones. The topographic height of CS-rGO increases to ~3 nm, revealing that CS chains have been successfully grafted onto the surface of GO sheets. It is also worth noting that GO sheets exist with very sharp edges and flat surfaces. In contrast, the edges of CS-rGO appear relatively coarse and some protuberances can be observed on the surfaces, which were mainly generated from the polymer wrapping and folding. The similar phenomenon has been widely unveiled in the recent studies on polymer-immobilized graphene sheets.[25−27]

In addition, the change in zeta potential according to pH variation is summarized in Figure 5. The zeta potential is

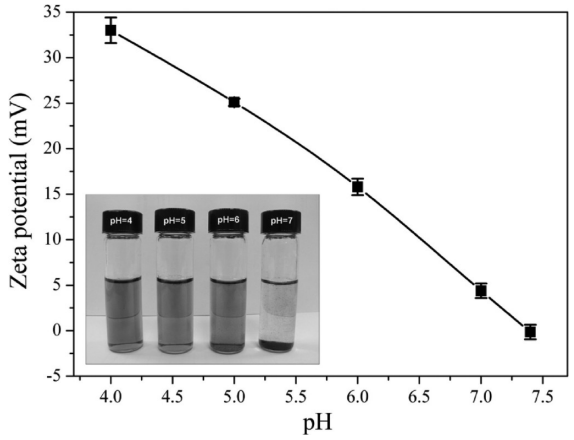

Figure 5. Zeta potential as a function of pH value for 0.2 mg/mL CS-rGO. The inset is the digital photo showing the long-term dispersion stability for 0.2 mg/mL CS-rGO in different pH valued solutions.

around +33 mV at pH 4 and it decreases continuously to +4.4 mV when pH value is increased to 7, which reflects the ongoing deprotonation process of the grafted CS. Finally, zeta potential approaching to 0 mV at pH 7.4 means the vanishing of electrostatic charge on the surface of CS-rGO. The inset photo shows the CS-rGO dispersions at different pH values and having stood for 3 days after sonication. At pH 4 and 5, the amino groups on CS chains are protonated and the CS-rGO composites can be dispersed well in aqueous solution due to the strong electrostatic repulsion. At pH 6, a majority of CS segments are deprotonated and the intra- and intermolecular repulsion decreases, resulting in the rolling up of the polymer chains. Without enough electrostatic repulsion force, these hydrophobic graphene sheets start to aggregate gradually. Upon pH reaching 7, entirely neutralized CS-rGO sheets precipitate

to the bottom on account of the hydrophobic association and strong hydrogen-bonding interactions.

3.2. MWCNT Exfoliations Using CS-G as a Dispersant.

In order to quantitatively assess the efficiency of CS-rGO in exfoliating MWCNTs, UV−vis spectroscopy was employed to detect the absorption of CS-rGO/MWCNT solutions under different conditions. Since bundled CNTs are rarely active in the wavelength range between 200 and 1200 nm and the absorption of individual CNTs become pronounced with increasing exfoliation, the dispersion extent of both MWCNTs[43,44] and SWCNTs[45,46] can be determined by their UV−vis absorption spectra. Through Bee-Lambert law (eq 1), we are able to establish a relationship between the exact concentrations of suspended MWCNTs and their absorbance values.

$$A = \varepsilon l c \quad (1)$$

where A is the absorbance at a particular wavelength (here we use 261 nm), ε is the extinction coefficient, l is the path length, and c is the concentration. The concentrations of MWCNTs in supernatants were estimated by measuring their dry weights and subtracting the CS-rGO weight. Figure 6A shows the UV−vis absorption spectra of CS-rGO/MWCNT solutions with different MWCNT concentrations at pH 4. The linear-least-squares fitting to the data gave a slope of 152, so the extinction coefficient of MWCNTs is 152 mL mg^{-1} cm^{-1}. As we used surfactant solutions with the same concentrations as MWCNTs as references in the tests, it can be assumed that the UV absorbance is solely due to the presence of dispersed MWCNTs. According to the extinction coefficient and the absorbance data, we can obtain the exact concentrations of dispersed MWNCTs in solutions.

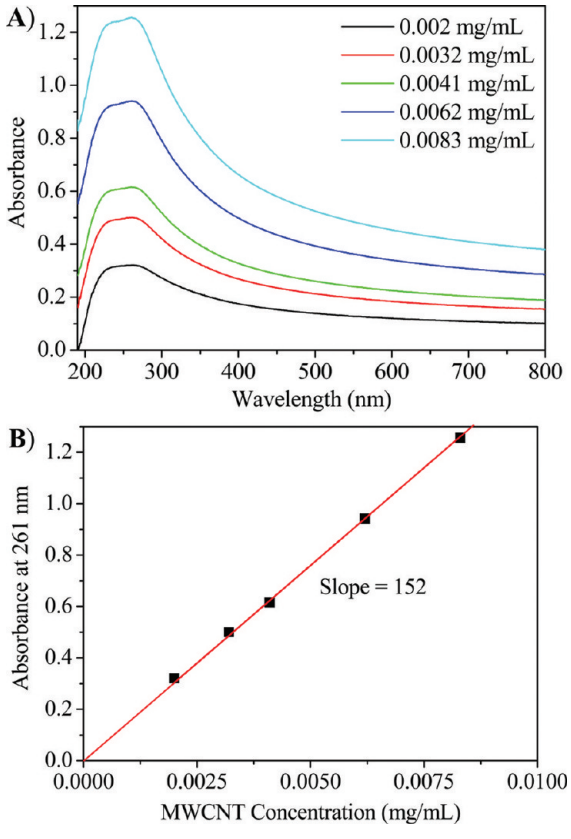

Figure 6. (A) UV−vis absorption spectra for CS-rGO/MWCNT aqueous solutions at pH 4 with different MWCNT concentrations and a fixed CS-rGO/MWCNT mass ratio of 1:1. (B) Calibration curve: absorbance at 261 nm versus MWCNT concentration in suspensions. The solutions were diluted by a factor of 100 when taking UV−vis measurements.

Figure 7A shows the concentrations of dispersed MWCNTs in CS-rGO/MWCNT solutions at different pH values and a

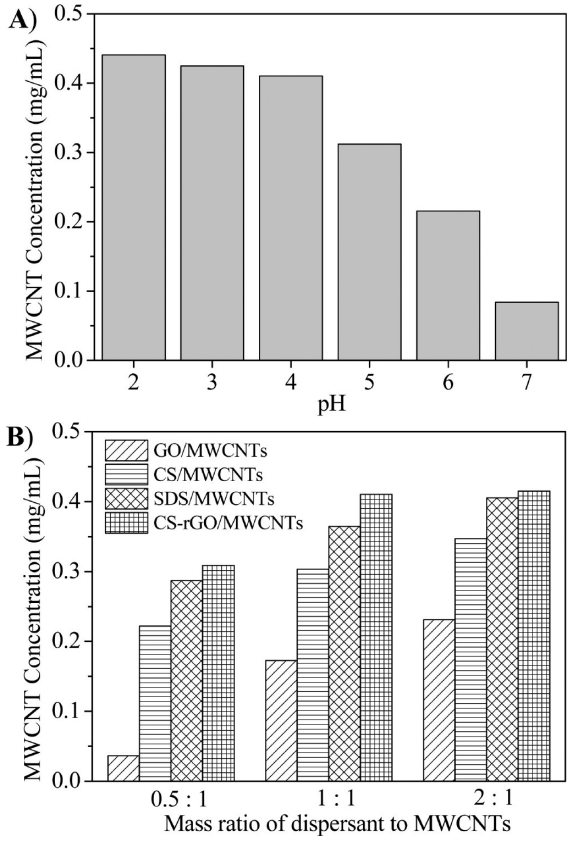

Figure 7. (A) Concentrations of MWCNTs dispersed in CS-rGO solutions at different pH values where CS-rGO to MWCNT mass ratio was 1:1. (B) MWCNT concentrations of solutions prepared using GO, CS, SDS or CS-rGO as a dispersant at three different mass ratios of dispersant to MWCNT.

CS-rGO to MWCNT mass ratio of 1:1. It is revealed that the amount of dispersed MWCNTs gradually decreased with increasing pH value because the solubility of CS-rGO itself was continuously decreasing in aqueous solutions with increasing pH value from 2 to 7. At pH values below 5, however, the concentrations of dispersed MWCNTs were relatively high and did not vary much with the change of pH value. Subsequently, we investigated the influence of mass ratio of CS-rGO to MWCNTs on the maximum concentration of MWCNTs to be dispersed. Three different ratios (0.5:1, 1:1 and 2:1) of CS-rGO/MWCNT were compared. To verify the efficacy of CS-rGO, we compared its ability to disperse MWCNTs with that of plain GO, pure CS, and SDS. SDS is a traditional surfactant for dispersing MWCNTs. Figure 7B presents the maximum concentrations of dispersed MWCNTs in the four dispersant solutions at different mass ratios of dispersant to MWCNTs, where the initial concentration of MWCNTs was fixed at 0.5 mg/mL. In general, with increasing the mass ratio of a dispersant to MWCNTs, the concentration of dispersed MWCNTs increases. Among the four dispersants, plain GO

exhibited the lowest capability of dispersing MWCNTs, whereas CS-rGO showed the highest capability of dispersing MWCNTs. For example, the concentration of dispersed MWCNTs at the mass ratio of CS-rGO: MWCNT = 0.5:1 was 0.31 mg/mL, which is more than 8 times and 2 times higher than the corresponding values of GO/MWCNT dispersion (0.037 mg/mL) and CS/MWCNT dispersion (0.15 mg/mL), respectively. The water solubility of GO is mainly attributed to the ionizable carboxyl groups on their edges. If immoderate amount of MWCNTs adhere to GO sheets, these MWCNTs tend to aggregate on the GO sheets, thus failing to maintain the dispersion stability in water. On the other hand, GO basal planes are only partially hydrophobic as stated previously, which restricts the total quantity of MWCNTs to be bound on GO sheets. Liu et al. studied GO sheet-assisted dispersing of MWCNTs in aqueous media and found that excessive MWCNTs on GO sheets may reduce the solubility of GO/MWCNT complexes, leading to a certain degree of aggregation when the GO to MWCNT mass ratio is 0.5:1.[16] Only when the ratio reached 2:1 or higher could a stable dispersion of GO/MWCNTs be formed. The similar conclusions were drawn from the studies carried out by Huang et al.[11] and Sun et al.[20] In contrast, more MWCNTs can be dispersed in CS-rGO/MWCNT solutions. At CS-rGO to MWCNT mass ratios of 0.5:1, 1:1 and 2:1, the maximum concentrations of dispersed MWCNTs are 0.31, 0.41, and 0.42 mg/mL, respectively, which are higher than those in the SDS/MWCNT system at the same mass ratios, indicating the higher efficacy of CS-rGO in dispersing of MWCNTs than the commercial dispersant SDS. The enhanced ability of CS-rGO to disperse MWCNTs should be ascribed to its unique physical properties. The grafted CS provides stronger repulsion force in the acidic aqueous media, enabling CS-rGO to disperse more MWCNTs and maintain a stable dispersion. On the other hand, as chemical reduction removed those oxygen-containing groups in GO basal planes, CS-rGO basal planes become entirely hydrophobic and possess lager overall area of π-conjugated aromatic domains to allow more MWCNTs to adhere to.

The morphology of CS-rGO dispersed MWCNTs was observed by both TEM and AFM. Viewing from the TEM images (Figure 8A, B), transparent GO sheets on top of carbon film are observed to appear like crumpled silk veils leading to a large accessible area for MWCNTs to adhere to. On top of the GO sheets, a certain quantity of spaghetti-like nanotubes is randomly attached, and all of them are separated into individual ones. Figure 8C shows an AFM image of CS-rGO/MWCNT complex, in which the CS-rGO pallet is several-hundred nanometers in lateral size and of a thickness around 3 nm, in agreement with the previous AFM observation. The AFM image also reveals that CNTs are attached on CS-rGO sheets, which is similar with the GO dispersed CNTs reported in some recent work.[12] Apparently, it is proved that CS-rGO can effectively disperse MWCNTs individually in acidic aqueous solutions via noncovalent interactions, which inspires us to make use of CS-rGO dispersed MWCNTs as a hybrid nanofiller to reinforce CS.

3.3. Mechanical Properties of Reinforced CS Films.

With intention to study the reinforcing effect of CS-rGO-MWCNTs, we compare the mechanical properties of CS-rGO-MWCNT/CS nanocomposites with those containing single-component fillers such as pristine MWCNTs, CS-grafted MWCNTs (CS-MWCNTs), GO, or CS-rGO, in which the filler loading is fixed at 1 wt %. All the results are plotted in

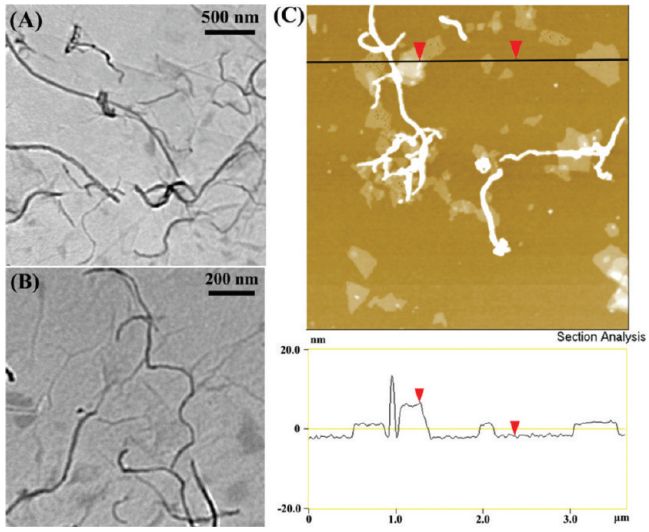

Figure 8. (A, B) TEM images of CS-rGO/MWCNTs under different magnifications; (C) AFM image with corresponding surface profile of CS-rGO/MWCNTs.

Figure 9 and summarized in Table 1. Note that the filler loading excludes the amount of CS for CS-MWCNTs, CS-rGO, and CS-rGO-MWCNTs and the ratio of rGO to MWCNTs was 1:1 for CS-rGO-MWCNTs.

To achieve larger improvements in the mechanical properties of polymer nanocomposites, several requirements should be fulfilled, which include good dispersion of nanoparticles, strong interfacial interactions between nanoparticles and matrix, as well as effective load transfer from nanoparticles to matrix. Herein, MWCNTs are able to be dispersed in acidic water by CS, and other nanoparticles like CS-MWCNTs, GO, CS-rGO, and CS-rGO-MWCNTs all have good compatibility with the CS matrix, so all of them can be well dispersed in the CS matrix. Therefore, the interfacial interactions and load transfer are supposed to be the essential factors accounting for the differences in mechanical properties of these nanocomposites. The nanoparticles incorporated into CS nanocomposites have different surface properties, which lead to their different interfacial interactions with the CS matrix.

Among all the samples containing fillers, the pristine MWCNT/CS nanocomposites have the poorest mechanical properties. With addition of 1 wt % pristine MWCNTs, the tensile modulus and strength of the nanocomposites increased by 38 and 47%, respectively, but the elongation at break decreased from 22.5 to 18.5%, making the toughness of MWCNT/CS nanocomposites only slightly higher than that of neat CS. Because the dispersion of MWCNTs is uniform and homogeneous (as observed from Figure 10A1), the relatively low reinforcing effect of pristine MWCNTs primarily results from the absence of strong interfacial adhesion between pristine MWCNTs and the CS matrix due to the inert surface of pristine MWCNTs. Some researchers attempted to introduce carboxyl groups onto the surfaces of MWCNTs so as to improve their interfacial adhesions with the hydrophilic CS matrix.[47,48] However, a limited amount of carboxyl groups could not change the overall hydrophobic property of MWCNTs, and the poor wetting of MWCNTs could hardly make the elongation at break of nanocomposites increase. In contrast, the grafted CS brings abundant polar groups and compatible CS chains with the CS matrix. As a result, the CS-

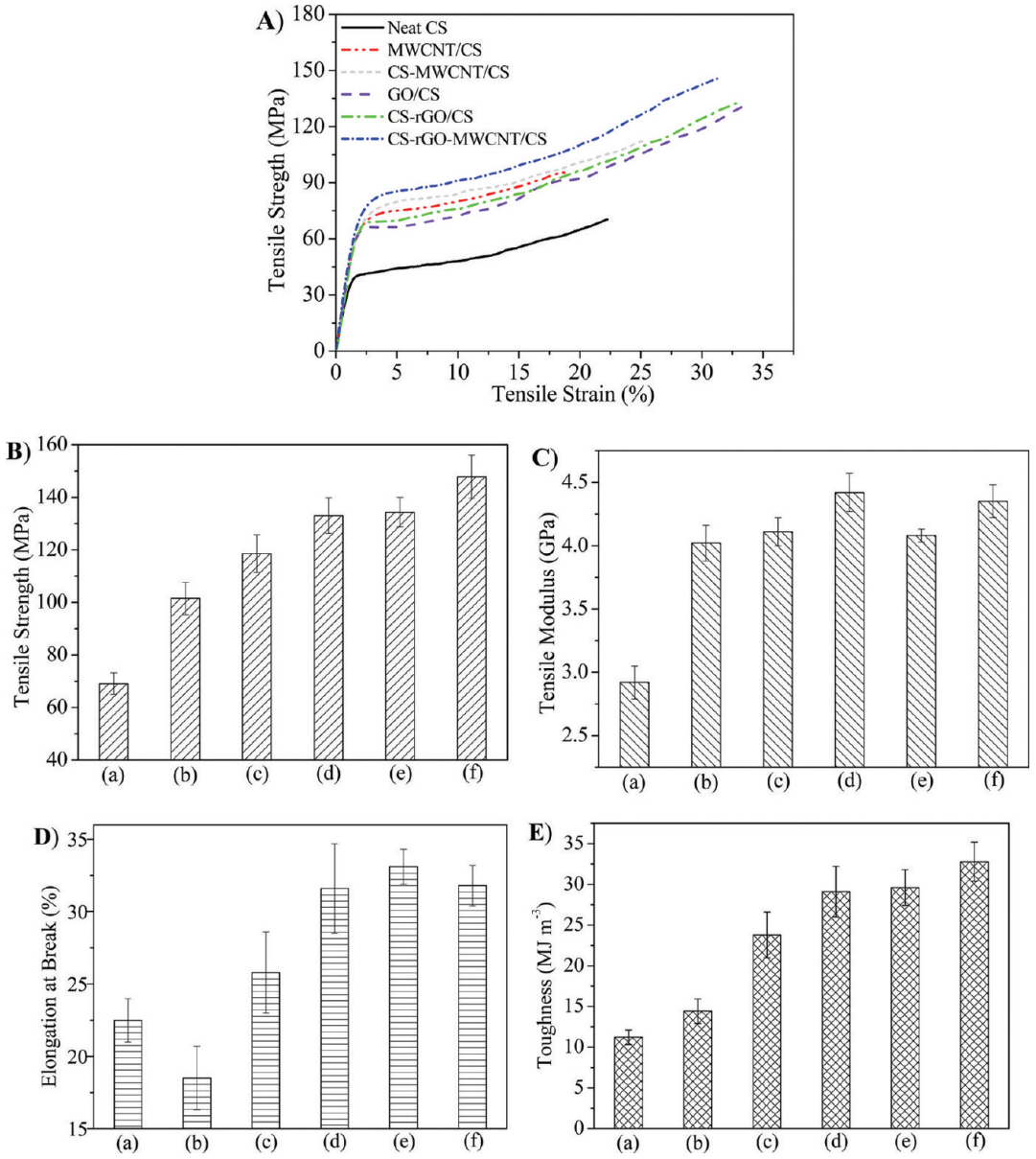

Figure 9. (A) Representative stress−strain curves, (B) tensile strength, (C) tensile modulus, (D) elongation at break, and (E) toughness of (a) neat CS, (b) 1 wt % MWCNT/CS, (c) 1 wt % CS-MWCNT/CS, (d) 1 wt % GO/CS, (e) 1 wt % CS-rGO/CS, and (f) 1 wt % CS-rGO-MWCNT/CS composites.

MWCNTs show a prominently improved toughening effect on the nanocomposites. The elongation at break and toughness increased by 15 and 112% compared to neat CS, respectively. As we reported previously, GO has been proved to be a good reinforcing and toughening agent for CS nanocomposites because of its hydrophilicity.[38] Similarly, because of the structural similarity and compatibility between grafted CS and the CS matrix, CS-rGO was also dispersed well and had strong interactions with the CS matrix. Consequently, CS-rGO/CS nanocomposites exhibit a comparable mechanical property with the GO/CS analogue. Finally, it is found the ability of the CS-rGO-MWCNTs to toughen the matrix is superior to the single-component fillers. With incorporation of 1 wt % CS-rGO-MWCNTs, the strength and toughness of the nanocomposites can be increased by 114% and 193%, respectively. The tensile reinforcing and toughening efficiency can also be quantitatively evaluated by calculating the tensile strength per unit weight fraction ($\Delta\sigma/\Delta W$). The $\Delta\sigma/\Delta W$ and dT/dW of 1 wt % CS-rGO-MWCNT/CS nanocomposites reach 7870 MPa. The value is superior not only to the results of other nanocompositess in this study but also to those CNT/CS and graphene/CS nanocomposites reported previously (see the Supporting Information, Table S2).[47−53]

The significant effect of CS-rGO-MWCNTs on reinforcing and toughening of CS stems from several reasons. First, as we mentioned above, the MWCNTs can be effectively dispersed by CS-rGO because of its favorable compatibility with the CS matrix, and the CS-rGO-MWCNTs are also dispersed quite homogeneously in CS nanocomposites. Second, there exist hydrophobic interactions between graphene sheets and carbon nanotubes. Third, the CS chains immobilized on the surface of graphene sheets are expected to form hydrogen bonds with the CS matrix, which lead to strong interfacial interactions. In addition, grafted CS is able to root into the CS matrix so that

Table 1. Mechanical Properties of Neat CS and CS Nanocomposites with Various Fillers at 1 wt % Filler Loading

sample	σ (MPa)	E (GPa)	ε (%)	T^a (MJ m^{-3})
neat CS	69.1 ± 4.1	2.92 ± 0.13	22.5 ± 1.5	11.2 ± 0.9
pristine MWNCT/CS	101.5 ± 6.2	4.02 ± 0.14	18.5 ± 2.2	13.4 ± 1.5
CS-MWCNT/CS	118.6 ± 7.2	4.11 ± 0.11	25.8 ± 2.8	23.8 ± 2.8
GO/CS[b]	133.1 ± 6.8	4.42 ± 0.15	31.6 ± 3.1	29.1 ± 3.1
CS-rGO/CS	134.4 ± 5.6	4.08 ± 0.05	33.1 ± 1.2	29.6 ± 2.2
CS-rGO-MWCNT/CS	147.8 ± 8.2	4.35 ± 0.13	31.8 ± 1.4	32.8 ± 2.4

[a]Calculated from the area under the stress−strain curve. [b]The data of GO/CS are cited from our previous work.[38]

the anchored CS-rGO-MWCNTs restrict mobility of adjacent CS.[54−56] The combination of these interactions jointly contributes to an effective load transfer between CS-rGO-MWCNTs and the CS matrix, thus enhancing the strength of nanocomposites. With regard to toughening effect, both CNTs and graphene can play special roles in toughening polymers due to their respective unique geometries and rigid structures. Because of the curled-fiber structure and high aspect ratio of MWCNTs, nanocomposites containing MWCNTs could form a fiber-bridging zone in the wake of the crack tip.[57] The frictional slide-out of the bridging nanotubes from the polymer matrix can slow down the crack propagation speed and dissipate energy. This mechanism is termed as crack bridging. On the other hand, the dominant toughening mechanism of graphene was based on crack deflection occurring, where an initial crack tilts and twists when it encounters rigid graphene nanoplatelets and hence passes around them.[57,58] In the CS-rGO-MWCNT/CS nanocomposites, MWCNTs are tightly bound onto the surface of graphene sheets and both of them are tangled with the CS matrix through strong interfacial interactions, so they are able to take effect to resist crack propagation upon crack growth under external force. The combination of these two crack-resisting effects can be achieved in the CS-rGO-MWCNT/CS system, as a consequence endowing the nanocomposites with a significantly improved toughness.

The fracture surface morphologies of the samples after tensile tests were observed by FESEM, which provide information on these interfacial interactions in the different nanocomposites. Figure 10 shows the images under different magnifications. It appears that all the fillers are dispersed well in the CS matrix and no aggregates can be discerned, but the surface morphologies of each sample vary significantly. For pristine MWCNT/CS nanocomposites (Figure 10A), many broken MWCNT segments with large length and the small holes left were observed as marked by arrows, indicating that most of MWCNTs were pulled out from the matrix rather than fractured under the imposed force. The poor wetting of MWCNTs and the weak interfacial interactions between MWCNTs and the CS bulk were proved. In the case of CS-MWCNT/CS nanocomposites (Figure 10B), some nanotubes appear to be partially pulled out from the surface but the pull-out lengths of MWCNTs significantly decrease (marked by squares in Figure 10B2), which probably resulted from the MWCNT failure in a sliding-fracture mode.[59] Other nanotubes were fractured at the fracture surface and the ends are embedded in the matrix (indicated by circles in Figure 10B2). The morphologies imply that the interfacial adhesion between CS-MWCNT and CS is stronger than that in pristine MWCNT/CS.

Viewing from Figure 10C, it is found that the CS-rGO sheets are imbedded into the polymer matrix homogeneously and almost all of them were fractured at the fracture surface rather than pulled out, confirming the good compatibility and strong interfacial adhesion between CS-rGO and the CS matrix. This morphology resembles what we observed for the GO/CS nanocomposites reported before. From the FESEM images of fracture surface of the CS-rGO-MWCNT/CS nanocomposite (Figure 10D), CS-rGO-MWCNTs are known to be dispersed homogeneously in the CS matrix without any aggregates, and both CS-rGO and MWCNTs appear to be broken at the fracture surface and tightly embedded in the matrix, suggesting the strong interfacial interactions between CS-rGO-MWCNTs and CS. CS-rGO sheets and MWCNTs are marked by dot circles and dash circles, respectively. The former owns thicknesses of less than ten nanometers and lateral lengths of several-hundred nanometers, and the latter possesses broken ends with diameters of 10−20 nm.

Because the G and G′ bands of CNT or graphene from Raman spectrum have been reported to increase with hydrostatic pressure and decrease under tension, Raman spectroscopy is widely used to investigate the interfacial stress transfer in polymer composites containing CNT or graphene.[60,61] Herein, to study the effect of CS-rGO-MWCNTs in reinforcing and toughening CS matrix, we employed Raman spectrocopy to study the undrawn and drawn composites containing 1 wt % CS-rGO-MWCNTs. The obtained Raman spectra of the composites at different strains and the G and G′ band downshifts as a function of strain are shown in Figure S1 in the Supporting Information. From Figure S1A, it is observed that the G and G′ bands of 1 wt % CS-rGO-MWCNT/CS without a strain (i.e., strain = 0%) are located at 1608.8 and 2683.4 cm^{-1}, respectively. With increasing strain from 0 to 10%, both of the two bands downshifted gradually. In the elastic region (strain <2%), they downshifted almost linearly with the applied strain (Figure S1B and C), which is in agreement with the empirical relationship reported in the literature.[62−64] The slopes of G and G′ band downshifts in this region are about −4.8 cm^{-1}/% strain and −12.4 cm^{-1}/% strain, respectively. The significant downshifts suggest that the external stress applied to the composites is effectively transferred onto the CS-rGO and MWCNTs, thus confirming the strong adhesion between CS-rGO-MWCNT and the CS matrix. Moreover, in the plastic region (strain >2%), it is found that both of the G and G′ bands still slightly downshifted with increasing strain, further indicating the effective load transfer between CS-rGO-MWCNT and CS, which existed not only in the elastic region but also in the plastic region. This result explains why the incorporation of CS-rGO-MWCNTs significantly increased the elongation at break and enhanced the toughness of the nanocomposites.

We have found that the reinforcing and toughening effects of CS-rGO-MWCNTs are much more prominent than those of single-component fillers, such as MWCNTs, GO, and CS-rGO. The synergistic effect results from not only the homogeneous dispersion of CS-rGO-MWCNTs, but also the effective load transfer among MWCNTs, CS-rGO, and CS matrix. Besides, the combination of different interacting natures of CS-rGO and

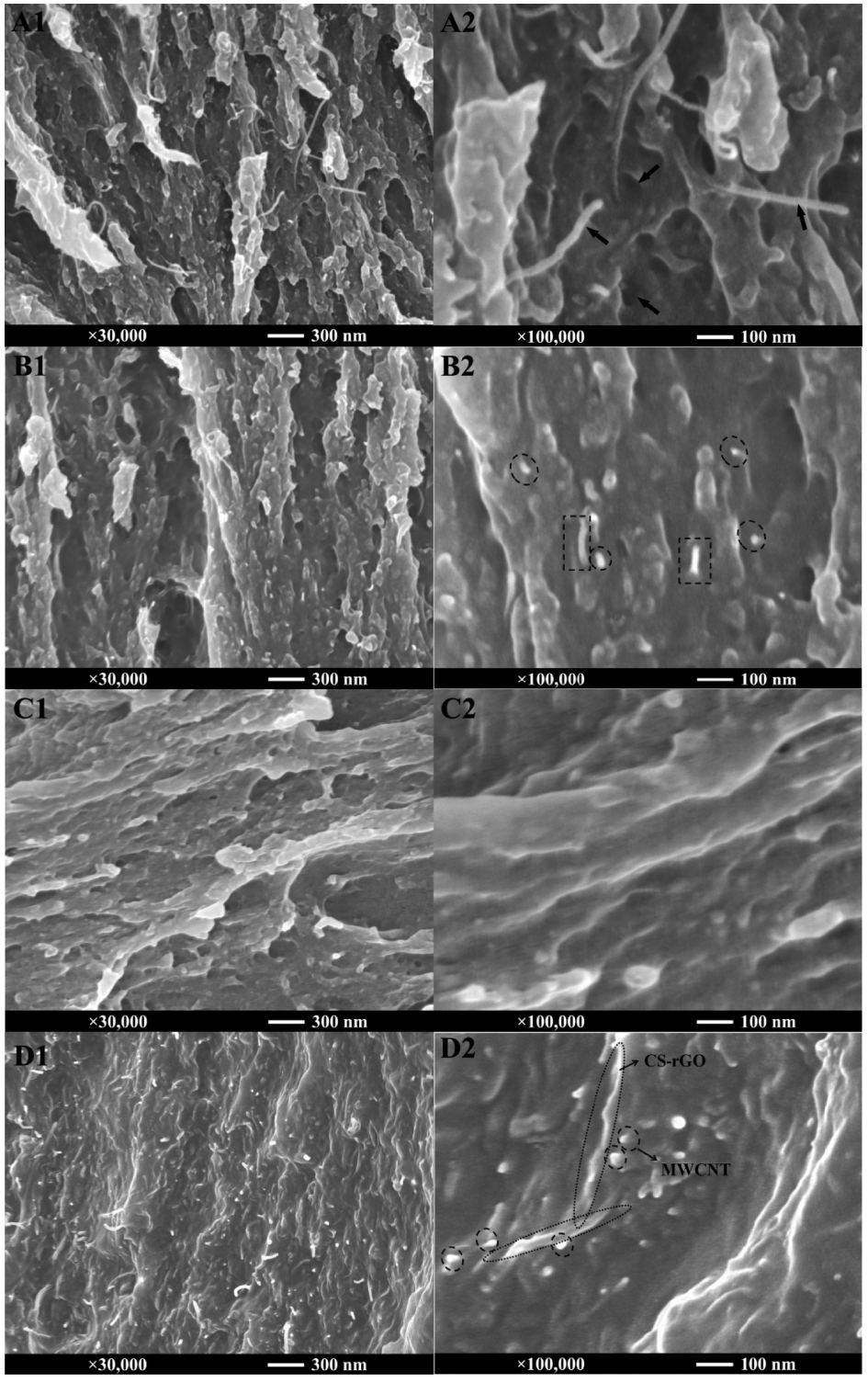

Figure 10. FESEM images of cross-sectional facture surfaces of (A) 1 wt % MWCNT/CS, (B) CS-MWCNT/CS, (C) CS-rGO/CS, and (D) CS-rGO-MWCNT/CS nanocomposites.

MWCNTs may also make some contribution to the synergistic effect.[65] The long and flexible MWCNTs can interact over the length of the CS chains, whereas CS-rGO with a two-dimensional structure has two sides that can both interact with the CS matrix. Thus, the CS-rGO-MWCNTs could have an enhanced contact surface area with the CS matrix compared to these single-component fillers, so inducing the remarkable synergistic effect. Herein, we propose a possible microstructure to illustrate the mechanism for the reinforcing and toughening effects of CS-rGO-MWCNTs on CS nanocomposites (shown in Scheme 2). First, MWCNTs are strongly bound to the graphene sheets via $\pi-\pi$ interaction and hydrophobic interaction (interaction 1). Second, graphene sheets are covalently linked to grafted CS chains (interaction 2). Finally, the strong hydrogen bonds between CS chains and the CS matrix widely exist in the interfacial zone and the grafted CS

Scheme 2. Proposed Microstructrure Present in a CS-rGO-MWCNT/CS Nanocomposite[a]

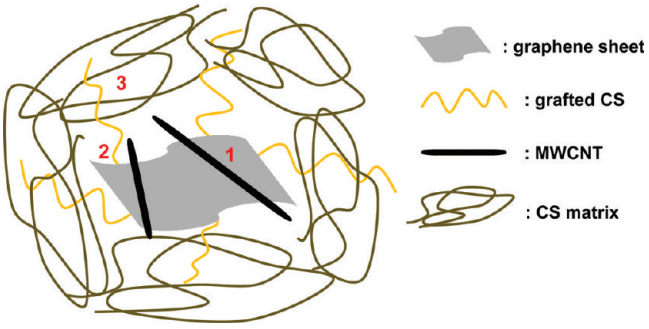

[a]The possible interactions in the composite could include: (1) interaction between graphene sheet and nanotubes, (2) covalent link between graphene sheets and grafted CS, and (3) hydrogen bonds between grafted CS and the CS matrix.

makes CS-rGO-MWCNTs anchored into the CS matrix (interaction 3). These factors are jointly responsible for the strong interfacial adhesions between CS-rGO-MWCNTs and the CS matrix, making CS-rGO-MWCNT/CS nanocomposites possess significantly enhanced strength and toughness.

4. CONCLUSIONS

In summary, we have developed a green and facile method to prepare soluble rGO sheets by functionalizing them with chitosan (CS). The chemical structure and morphology of the synthesized CS-rGO were characterized by FTIR, UV−vis, Raman spectroscopy, XPS and AFM. CS-rGO had a superior capability in dispersing and stabilizing MWCNTs in acidic aqueous solutions via noncovalent interactions. UV−vis spectroscopy quantitatively assessed the efficiency of CS-rGO in dispersing MWCNTs. When the mass ratio of the CS-rGO to MWCNTs was 1:1 and the initial concentration of MWCNTs was 0.5 mg/mL, the dispersed concentration of MWCNTs after 30 min sonication could reach 0.41 mg/mL, which is much higher than the values obtained in GO or SDS dispersed MWCNT solutions under the same condition. Subsequently, the CS-rGO dispersed MWCNTs were used to reinforce the CS in its nanocomposites and the reinforcement was compared with the nanocomposites containing pristine MWCNTs, CS-MWCNTs, GO and CS-rGO. It was found that CS-rGO-MWCNTs remarkably outperformed the other fillers for reinforcing and toughening of CS. With incorporation of 1 wt % CS-rGO-MWCNTs, the tensile modulus, strength and toughness of the nanocomposites could be increased by 49, 114, and 193%, respectively. Raman spectroscopic characterization was employed to verify the effective load transfer between CS-rGO-MWCNTs and the CS matrix, which was considered as the main reason for the simultaneously increased strength and toughness of the nanocomposites. The load transfer was attributed to three kinds of interfacial interactions: interaction between graphene sheet and nanotubes, covalent bond between graphene sheets and grafted CS, and hydrogen bonds between grafted CS and the CS matrix.

■ ASSOCIATED CONTENT

Supporting Information

Preparation of CS-grafted MWCNTs (CS-MWCNTs) and MWCNT/chitosan nanocomposites; atomic and mass concentrations of C, N, and O elements in GO, CS, CS-GO, CS-rGO ,and rGO; comparison of our tensile properties with reported data of CNT/CS and graphene/CS nanocomposites; Raman spectrum results of the 1 wt % CS-rGO-MWCNT/CS composites under different strains. This material is available free of charge via the Internet at http://pubs.acs.org/.

■ AUTHOR INFORMATION

Corresponding Author

*Tel.: +65-6790 6285. Fax: +65-6791 1859. E-mail: mlli@ntu.edu.sg (Lin Li).

■ REFERENCES

(1) Geim, A. K. *Science* **2009**, *324*, 1530−1534.
(2) Allen, M. J.; Tung, V. C.; Kaner, R. B. *Chem. Rev.* **2010**, *110*, 132−145.
(3) Rao, C. N. R.; Sood, A. K.; Subrahmanyam, K. S.; Govindaraj, A. *Angew. Chem., Int. Ed.* **2009**, *48*, 7752−7777.
(4) Stankovich, S.; Dikin, D. A.; Piner, R. D.; Kohlhaas, K. A.; Kleinhammes, A.; Jia, Y.; Wu, Y.; Nguyen, S. T.; Ruoff, R. S. *Carbon* **2007**, *45*, 1558−1565.
(5) Dreyer, D. R.; Park, S.; Bielawski, C. W.; Ruoff, R. S. *Chem. Soc. Rev.* **2010**, *39*, 228−240.
(6) Che, J.; Shen, L.; Xiao, Y. *J. Mater. Chem.* **2010**, *20*, 1722−1727.
(7) Oh, J.; Lee, J. H.; Koo, J. C.; Choi, H. R.; Lee, Y.; Kim, T.; Luong, N. D.; Nam, J. D. *J. Mater. Chem.* **2010**, *20*, 9200−9204.
(8) Chen, S. S.; Brown, L.; Levendorf, M.; Cai, W. W.; Ju, S. Y.; Edgeworth, J.; Li, X. S.; Magnuson, C. W.; Velamakanni, A.; Piner, R. D.; Kang, J. Y.; Park, J.; Ruoff, R. S. *ACS Nano* **2011**, *5*, 1321−1327.
(9) Fang, M.; Zhang, Z.; Li, J. F.; Zhang, H. D.; Lu, H. B.; Yang, Y. L. *J. Mater. Chem.* **2010**, *20*, 9635−9643.
(10) Kim, F.; Cote, L. J.; Huang, J. X. *Adv. Mater.* **2010**, *22*, 1954−1958.
(11) Kim, J.; Cote, L. J.; Kim, F.; Yuan, W.; Shull, K. R.; Huang, J. X. *J. Am. Chem. Soc.* **2010**, *132*, 8180−8186.
(12) Tung, V. C.; Huang, J.-H.; Tevis, I.; Kim, F.; Kim, J.; Chu, C.-W.; Stupp, S. I.; Huang, J. *J. Am. Chem. Soc.* **2011**, *133*, 4940−4947.
(13) Wang, R. R.; Sun, J.; Gao, L. A.; Xu, C. H.; Zhang, J.; Liu, Y. Q. *Nanoscale* **2011**, *3*, 904−906.
(14) Cote, L. J.; Kim, J.; Tung, V. C.; Luo, J. Y.; Kim, F.; Huang, J. X. *Pure Appl. Chem.* **2011**, *83*, 95−110.
(15) Gudarzi, M. M.; Sharif, F. *Soft Matter* **2011**, *7*, 3432−3440.
(16) Zhang, C.; Ren, L. L.; Wang, X. Y.; Liu, T. X. *J. Phys. Chem. C* **2010**, *114*, 11435−11440.
(17) Tian, L.; Anilkumar, P.; Cao, L.; Kong, C. Y.; Meziani, M. J.; Qian, H.; Veca, L. M.; Thorne, T. J.; Tackett, K. N.; Edwards, T.; Sun, Y. P. *Acs Nano* **2011**, *5*, 3052−3058.
(18) Song, X.; Yang, Y.; Liu, J.; Zhao, H. *Langmuir* **2010**, *27*, 1186−1191.
(19) Zhang, W. L.; Liu, Y. D.; Choi, H. J. *J. Mater. Chem.* **2011**, *21*, 6916−6921.
(20) Tian, L. L.; Meziani, M. J.; Lu, F. S.; Kong, C. Y.; Cao, L.; Thorne, T. J.; Sun, Y. P. *ACS Appl. Mater. Interfaces* **2010**, *2*, 3217−3222.
(21) Li, D.; Muller, M. B.; Gilje, S.; Kaner, R. B.; Wallace, G. G. *Nat. Nanotechnol.* **2008**, *3*, 101−105.
(22) Loh, K. P.; Bao, Q. L.; Ang, P. K.; Yang, J. X. *J. Mater. Chem.* **2010**, *20*, 2277−2289.
(23) Sun, Y. Q.; Wu, Q. O.; Xu, Y. X.; Bai, H.; Li, C.; Shi, G. Q. *J. Mater. Chem.* **2011**, *21*, 7154−7160.
(24) Salavagione, H. J.; Martinez, G. *Macromolecules* **2011**, *44*, 2685−2692.
(25) Stankovich, S.; Piner, R. D.; Chen, X. Q.; Wu, N. Q.; Nguyen, S. T.; Ruoff, R. S. *J. Mater. Chem.* **2006**, *16*, 155−158.
(26) Liu, S.; Tian, J. Q.; Wang, L.; Li, H. L.; Zhang, Y. W.; Sun, X. P. *Macromolecules* **2010**, *43*, 10078−10083.
(27) Fang, M.; Wang, K. G.; Lu, H. B.; Yang, Y. L.; Nutt, S. *J. Mater. Chem.* **2009**, *19*, 7098−7105.
(28) Kan, L. Y.; Xu, Z.; Gao, C. *Macromolecules* **2011**, *44*, 444−452.

(29) Yang, H.; Zhang, Q.; Shan, C.; Li, F.; Han, D.; Niu, L. *Langmuir* **2010**, *26*, 6708−6712.
(30) Park, S.; Mohanty, N.; Suk, J. W.; Nagaraja, A.; An, J. H.; Piner, R. D.; Cai, W. W.; Dreyer, D. R.; Berry, V.; Ruoff, R. S. *Adv. Mater.* **2010**, *22*, 1736−1740.
(31) Shan, C. S.; Yang, H. F.; Han, D. X.; Zhang, Q. X.; Ivaska, A.; Niu, L. *Langmuir* **2009**, *25*, 12030−12033.
(32) Hsiao, M. C.; Liao, S. H.; Lin, Y. F.; Wang, C. A.; Pu, N. W.; Tsai, H. M.; Ma, C. C. M. *Nanoscale* **2011**, *3*, 1516−1522.
(33) Sahoo, N. G.; Bao, H.; Pan, Y.; Pal, M.; Kakran, M.; Cheng, H. K. F.; Li, L.; Tan, L. P. *Chem. Commun.* **2011**, *47*, 5235−5237.
(34) Bao, H. Q.; Pan, Y. Z.; Ping, Y.; Sahoo, N. G.; Wu, T. F.; Li, L.; Li, J.; Gan, L. H. *Small* **2011**, *7*, 1569−1578.
(35) Pan, Y.; Bao, H.; Sahoo, N. G.; Wu, T.; Li, L. *Adv. Funct. Mater.* **2011**, *21*, 2754−2763.
(36) Hummers, W. S.; Offeman, R. E. *J. Am. Chem. Soc.* **1958**, *80*, 1339−1339.
(37) Kovtyukhova, N. I.; Ollivier, P. J.; Martin, B. R.; Mallouk, T. E.; Chizhik, S. A.; Buzaneva, E. V.; Gorchinskiy, A. D. *Chem. Mater.* **1999**, *11*, 771−778.
(38) Pan, Y.; Wu, T.; Bao, H.; Li, L. *Carbohydr. Polym.* **2011**, *83*, 1908−1915.
(39) Fernandez-Merino, M. J.; Guardia, L.; Paredes, J. I.; Villar-Rodil, S.; Solis-Fernandez, P.; Martinez-Alonso, A.; Tascon, J. M. D. *J. Phys. Chem. C* **2010**, *114*, 6426−6432.
(40) Dua, V.; Surwade, S. P.; Ammu, S.; Agnihotra, S. R.; Jain, S.; Roberts, K. E.; Park, S.; Ruoff, R. S.; Manohar, S. K. *Angew. Chem., Int. Ed.* **2010**, *49*, 2154−2157.
(41) Paredes, J. I.; Villar-Rodil, S.; Martinez-Alonso, A.; Tascon, J. M. D. *Langmuir* **2008**, *24*, 10560−10564.
(42) Fang, M.; Long, L. A.; Zhao, W. F.; Wang, L. W.; Chen, G. H. *Langmuir* **2010**, *26*, 16771−16774.
(43) Yu, J. R.; Lu, K. B.; Sourty, E.; Grossiord, N.; Konine, C. E.; Loos, J. C. *Carbon* **2007**, *45*, 2897−2903.
(44) Rausch, J.; Zhuang, R. C.; Mader, E. *Composites, Part A* **2010**, *41*, 1038−1046.
(45) Yuan, W.; Feng, J. L.; Judeh, Z.; Dai, J.; Chan-Park, M. B. *Chem. Mater.* **2010**, *22*, 6542−6554.
(46) Grossiord, N.; Regev, O.; Loos, J.; Meuldijk, J.; Koning, C. E. *Anal. Chem.* **2005**, *77*, 5135−5139.
(47) Tang, C. Y.; Xiang, L. X.; Su, J. X.; Wang, K.; Yang, C. Y.; Zhang, Q.; Fu, Q. *J. Phys. Chem. B* **2008**, *112*, 3876−3881.
(48) Wang, S. F.; Shen, L.; Zhang, W. D.; Tong, Y. J. *Biomacromolecules* **2005**, *6*, 3067−3072.
(49) Wang, X. L.; Bai, H.; Yao, Z. Y.; Liu, A. R.; Shi, G. Q. *J. Mater. Chem.* **2010**, *20*, 9032−9036.
(50) Cao, X. D.; Dong, H.; Li, C. M.; Lucia, L. A. *J. Appl. Polym. Sci.* **2009**, *113*, 466−472.
(51) Liu, Y. L.; Chen, W. H.; Chang, Y. H. *Carbohydr. Polym.* **2009**, *76*, 232−238.
(52) Yang, X. M.; Tu, Y. F.; Li, L. A.; Shang, S. M.; Tao, X. M. *ACS Appl. Mater. Interfaces* **2010**, *2*, 1707−1713.
(53) Han, D. L.; Yan, L. F.; Chen, W. F.; Li, W. *Carbohydr. Polym.* **2011**, *83*, 653−658.
(54) Rittigstein, P.; Priestley, R. D.; Broadbelt, L. J.; Torkelson, J. M. *Nat. Mater.* **2007**, *6*, 278−282.
(55) Potts, J. R.; Lee, S. H.; Alam, T. M.; An, J.; Stoller, M. D.; Piner, R. D.; Ruoff, R. S. *Carbon* **2011**, *49*, 2615−2623.
(56) Qiao, R.; Brinson, L. C. *Compos. Sci. Technol.* **2009**, *69*, 491−499.
(57) Rafiee, M. A.; Rafiee, J.; Wang, Z.; Song, H. H.; Yu, Z. Z.; Koratkar, N. *Acs Nano* **2009**, *3*, 3884−3890.
(58) Johnsen, B. B.; Kinloch, A. J.; Mohammed, R. D.; Taylor, A. C.; Sprenger, S. *Polymer* **2007**, *48*, 530−541.
(59) Tang, L. C.; Zhang, H.; Wu, X. P.; Zhang, Z. *Polymer* **2011**, *52*, 2070−2074.
(60) Schadler, L. S.; Giannaris, S. C.; Ajayan, P. M. *Appl. Phys. Lett.* **1998**, *73*, 3842−3844.
(61) Zhang, X. F.; Liu, T.; Sreekumar, T. V.; Kumar, S.; Moore, V. C.; Hauge, R. H.; Smalley, R. E. *Nano Lett.* **2003**, *3*, 1285−1288.
(62) Lachman, N.; Bartholome, C.; Miaudet, P.; Maugey, M.; Poulin, P.; Wagner, H. D. *J. Phys. Chem. C* **2009**, *113*, 4751−4754.
(63) Srivastava, I.; Mehta, R. J.; Yu, Z. Z.; Schadler, L.; Koratkar, N. *Appl. Phys. Lett.* **2011**, *98*, 063102.
(64) Li, J.; Gao, Y.; Ma, W.; Liu, L.; Zhang, Z.; Niu, Z.; Ren., Y.; Zhang, X.; Zeng, Q.; Dong, H.; Zhao, D.; Cai, L.; Zhou, W.; Xie, S. *Nanoscale* **2011**, *3*, 3731−3736.
(65) Prasad, K. E.; Das, B.; Maitra, U.; Ramamurty, U.; Rao, C. N. R. *Proc. Natl. Acad. Sci., U.S.A.* **2009**, *106*, 13186−13189.